Available online at www.easd.procedia.org
EASD Procedia EURODYN (2026) 2506-2518

EASD Procedia

EURODYN 2026
XIII International Conference on Structural Dynamics
M. Beer, C. Papadimitriou, H. Jensen, J. Chen, M. Broggi, J. Behrensdorf (eds.)
Hannover, Germany, 27.09.–01.10.2026

FEATURE RECONSTRUCTION AND MONITORING OF LOAD TEST DATA UNDER VARYING ENVIRONMENTAL CONDITIONS

Lizzie Neumann[1], Philipp Wittenberg[1], Alexander Mendler[2], and Jan Gertheiss[1]

[1]Chair of Statistics and Data Science
Dept. of Mathematics and Statistics
School of Business, Economics and Social Sciences
Helmut Schmidt University
Hamburg, Germany
e-mail: {neumannl,pwitten,gertheij}@hsu-hh.de

[2]Chair of Non-destructive Testing
Dept. of Materials Engineering
TUM School of Engineering and Design
Technical University of Munich
Munich, Germany
e-mail: alexander.mendler@tum.de

Keywords: Conditional covariance, Feature reconstruction, Kernel method, MEWMA control chart, Principal component analysis, Supervised Learning, Temperature removal.

Abstract. *System outputs in Structural Health Monitoring (SHM), such as sensor measurements or extracted features like eigenfrequencies, are influenced not only by (potential) damage but also by environmental and operational parameters (EOP). Identifying these variables and removing their effects from the data is essential before proceeding with further analysis. Most existing methods for this task focus on the expected values of system outputs, e.g., using different types of response surface modeling. However, it has been shown that confounding variables can also affect the (co-)variance of and between system outputs. This is particularly important because the covariance matrix is an essential building block in many damage detection methods in SHM. Beyond standard response surface modeling, a nonparametric kernel approach can be used to estimate a conditional covariance matrix that varies with the identified confounding parameter. This improves our understanding of how, for example, temperature affects the system's outputs.*

In this work, we present a new confounder-adjusted version of feature reconstruction. It uses the conditional covariance matrix as the basis for (conditional) principal component analysis. The resulting (conditional) principal component scores are then used to reconstruct system outputs with the confounding influences removed. In particular, the new approach eliminates the confounder's effect on both the mean and the covariance. As will be shown on load test data from the Vahrendorfer Stadtweg bridge in Hamburg, Germany, the reconstructed features can then be employed for monitoring, e.g., using an appropriate control chart, resulting in fewer false alarms and a higher probability of detecting damage.

ISSN:2311-9020 © 2026 The Authors. Published by EASD Procedia.
Peer-review under responsibility of the Organizing Committee of EURODYN 2026.
doi: 10.47964/1326.10846.088

1 INTRODUCTION

In structural health monitoring (SHM), structures such as bridges and buildings are tracked over time using regularly recorded measurements to detect changes in their material and geometric properties. Before anomalies can be detected, the effects of environmental and operational parameters (EOP) have to be removed from system outputs, such as sensor measurements or derived features. This process is known as "data normalization" [1] and there are various literature reviews available [2–4]. If a physically meaningful feature is reconstructed, data normalization is also called "feature reconstruction". Data normalization is essential because EOP can cause false alarms in damage detection. There are several data normalization methods that can be divided into two groups: "explicit" and "implicit" methods, depending on whether EOP must be measured. Implicit methods comprise, e.g., various types of principal component analysis (PCA) [5, 6], auto-associative neural networks [7], or non-parametric machine learning [8]. Explicit methods include, e.g., "response surface models" [9], methods using support vector machines [10], or neural networks [11]. What all these methods have in common is that they focus solely on the expected (mean) values of the system outputs and ignore the EOP's effects on measurement error. But [12] showed that not only the mean but also second-order statistical moments of system outputs need to be adjusted for EOP; in particular, accounting for changing temperatures is essential. For doing so, [12] developed a conditional version of PCA (thus, turning it into an explicit method). This approach can also be used for reconstructing physically meaningful features that are no longer influenced by temperature in the mean and covariance [13]. In this paper, the approach is applied to the load test data of the Vahrendorfer Stadtweg bridge.

The remainder of the paper is organized as follows. Section 2 presents the Vahrendorfer Stadtweg bridge and data set used for analysis. Section 3.1 discusses conditional principal component analysis (cPCA) using conditional covariances, confounder-adjusted feature reconstruction, and control charts for monitoring. Section 4 applies the proposed method to load test data from the Vahrendorfer Stadtweg bridge and compares it to two existing methods. The analysis shows that the new method outperforms existing methods and reliably detects additional masses placed on the bridge, whereas the other methods fail to do so. Section 5 concludes the paper.

2 LOAD TESTS ON THE VAHRENDORFER STADTWEG BRIDGE

In this paper, conditional PCA-based feature reconstruction will be applied to data from a real-world bridge, the "Vahrendorfer Stadtweg" bridge, where strain measurements will be analyzed. The outputs will be reconstructed for both in-control and out-of-control data to demonstrate that the confounding effect of temperature is removed, while the "damage" remains detectable.

The prestressed concrete bridge "Vahrendorfer Stadtweg" is a 50-meter-long and 10-meter-wide structure constructed in 1972; see Figure 1 (top left and middle). It spans the A7 freeway in the south of Hamburg, Germany, and features a single lane for agricultural traffic and a pedestrian walkway on the southeastern side. The bridge was built with an open frame design and a box girder cross-section. The analysis presented here used measurements from six strain sensors (in the z-direction) and one material temperature sensor. The sampling frequency of 200 Hz resp. 10 Hz was downsampled (averaged) to one measurement per hour, compare [3]. The sensor placement is shown in Figure 1 (bottom). Load tests were performed on the bridge between February 22nd and March 23rd, 2024. These tests involved three large bags filled with sand, weighing 680 kg, 740 kg, and 740 kg, respectively. The bags were placed in the middle of



Figure 1: Vahrendorfer Stadtweg bridge view from the north (top-left). Three additional masses at the middle of the bridge (top-right). Overview of sensor positions (bottom).

the bridge. Each extra mass was placed for 10 days and gradually increased in steps to 680 kg (scenario A), 1,420 kg (scenario B), and 2,160 kg (scenario C). Figure 1 (top right) shows the maximum mass (all three bags). Afterward, the masses were positioned at the quarter point of the south side, and truck crossings were conducted; however, this second measurement period will not be included in the analysis reported here. For a more detailed description of the bridge and the load tests, see [14].

3 METHODOLOGY

3.1 CONDITIONAL PRINCIPAL COMPONENT ANALYSIS AND FEATURE RECONSTRUCTION

In SHM, principal component analysis (PCA) is often employed for data normalization [6] and feature extraction [15, 16]. The first principal components often capture EOP, such as temperature [17], whereas PCA features with smaller eigenvalues demonstrate robustness to environmental variations [18]. So, the idea is to omit the leading principal components to remove the effects of EOP on the data. One challenge, however, is the uncertainty about the number of components to exclude. Excluding too few may result in residual environmental effects, whereas excluding too many may lead to the loss of crucial information about damage. Moreover, it remains uncertain whether this implicit approach can completely mitigate the influence of EOP, such as temperature variations [12, 19]. Consequently, accounting for confounding variables more explicitly may be a more effective strategy.

Standard PCA is an implicit, unsupervised machine learning tool that can be performed via an eigendecomposition of the covariance matrix of the system outputs alone. But if, instead of the marginal covariance matrix, a conditional covariance matrix $\mathbf{\Sigma}(z)$ is used, with the covariance varying with the confounding variable z, PCA becomes an explicit method. So, let $\mathbf{x} = (x_1, \ldots, x_p)^\top \in \mathbb{R}^p$ be a p-dimensional random (output) vector and $z \in \mathbb{R}$ a potential

confounder, then the *conditional* PCA can be carried out through [12]

$$\mathbf{\Sigma}(z) = \mathbf{A}(z)\mathbf{\Lambda}(z)\mathbf{A}(z)^\top, \tag{1}$$

with $\lambda_1(z), \ldots, \lambda_p(z)$ being the conditional eigenvalues and $\mathbf{a}_1(z), \ldots, \mathbf{a}_p(z)$ the conditional eigenvectors, which correspond to the (conditional) principal components. Note that the eigenvalues and eigenvectors can vary for different z, but conditional PCA requires the confounder to be measured. The conditional covariance matrix $\mathbf{\Sigma}(z)$ of $\mathbf{x}$ given a confounder z used in Eq. (1) can be estimated through [12, 20]

$$\hat{\mathbf{\Sigma}}(z; h) = \left\{ \sum_{i=1}^{n} K_h(z_i - z) \left[\mathbf{x}_i - \hat{\mathbf{m}}(z_i)\right] \left[\mathbf{x}_i - \hat{\mathbf{m}}(z_i)\right]^\top \right\} \left\{ \sum_{i=1}^{n} K_h(z_i - z) \right\}^{-1}, \tag{2}$$

where $\mathbf{x}_i = (x_{i1}, \ldots, x_{ip})^\top$, $i = 1, \ldots, n$, are observations of $\mathbf{x}$, z_i is the associated confounder variable (e.g., temperature), and $\hat{\mathbf{m}}(z_i)$ is an estimate of the mean of $\mathbf{x}$ at z_i. The conditional mean can, for instance, be estimated using methods such as penalized regression splines [21, 22], local polynomial regression [23] or a Nadaraya-Watson kernel estimator [12, 20]. $K_h(\cdot)$ is a kernel function with bandwidth h, with the latter being the smoothing parameter. The higher h, the wider the kernel and the smoother the estimated covariance function. The optimal bandwidth h can be estimated using cross-validation, as, e.g., described in [12, 13, 20, 24].

The eigenvalues and principal components from Eq. (1) can be used for *feature reconstruction*. First, the corresponding scores [12]

$$\mathbf{s}_i = (\mathbf{x}_i - \hat{\mathbf{m}}(z_i))^\top \mathbf{A}(z_i)(\mathbf{\Lambda}(z_i))^{-1/2}, \tag{3}$$

with $(\mathbf{\Lambda}(z_i))^{-1/2} = \mathrm{diag}(\lambda_1^{-1/2}(z_i), \ldots, \lambda_p^{-1/2}(z_i))$ are extracted. Using the (estimated) conditional mean $\hat{\mathbf{m}}(z_i)$, eigenvalues $\mathbf{\Lambda}(z_i)$, and principal components $\mathbf{A}(z_i)$ removes the effect of the confounder z from the component scores. These scores are uncorrelated, standardized quantities with a mean of zero and a variance of one for any given z-value [12, 19].

Then, the calculated scores $\mathbf{s}_i$ can be used to reconstruct the output data on the original, physically meaningful scale, with the confounder effect removed. Specifically, we have [13]

$$\tilde{\mathbf{x}}_i = \bar{\mathbf{x}} + \mathbf{A}(\mathbf{\Lambda})^{1/2}\mathbf{s}_i^\top, \tag{4}$$

with $\bar{\mathbf{x}}$ the marginal mean of $\mathbf{x}$, and $(\mathbf{\Lambda})^{1/2} = \mathrm{diag}(\lambda_1^{1/2}, \ldots, \lambda_p^{1/2})$ the eigenvalues and $\mathbf{A} = [\mathbf{a}_1 \ldots \mathbf{a}_p]$ the principal components from common PCA of the residual data, i.e., the (estimated) conditional mean given the confounder values had been subtracted from the measurements. The covariance of the residuals is also known under the name *partial* covariance. The marginal mean $\bar{\mathbf{x}}$ and partial eigenvalues and principal components are used for back-transforming instead of the conditional ones to prevent re-inducing the confounder effect removed in Eq. (3). Standard marginal PCA is not used in Eq. (4) because the first principal component(s) mainly account(s) for EOP, resulting in larger leading eigenvalues and over-weighting of the first component(s), which increases variation in the reconstructed output.

3.2 CONTROL CHARTS

The reconstructed features can be monitored using an appropriate control chart. Here, a multivariate memory-type control chart, the "Multivariate Exponentially Weighted Moving Average" (MEWMA) [25] is used to monitor the reconstructed output data from Eq. (4), under

the assumption that $\tilde{\mathbf{x}}_i \sim \mathcal{N}(\boldsymbol{\mu}, \boldsymbol{\Gamma})$. This type of control chart also incorporates past information, thereby increasing its sensitivity to small shifts.

First, a mean vector is defined based on a change point model, specifically, $\boldsymbol{\mu} = \boldsymbol{\mu}_0$ if $i < \vartheta$ and $\boldsymbol{\mu} = \boldsymbol{\mu}_1$ if $i \geq \vartheta$ for an unknown time point ϑ [26]. Then, with smoothing parameter $0 < \kappa \leq 1$, a smoothing procedure is applied to estimate the MEWMA statistic

$$\boldsymbol{\omega}_i = (1 - \kappa)\boldsymbol{\omega}_{i-1} + \kappa\tilde{\mathbf{x}}_i, \quad \boldsymbol{\omega}_0 = \mathbf{0}, \tag{5}$$

for time point $i = 1, 2, \ldots$. The smoothing parameter κ controls the sensitivity of the shift to be detected, i.e., smaller values such as $\kappa \in \{0.1, 0.2, 0.3\}$ are usually selected to detect smaller shifts [27], whereas $\kappa = 1$ results in the Hotelling chart [28]. The control statistic is the Mahalanobis distance

$$T_i^2 = (\boldsymbol{\omega}_i - \boldsymbol{\mu}_0)^\top \boldsymbol{\Gamma}_\omega^{-1} (\boldsymbol{\omega}_i - \boldsymbol{\mu}_0), \tag{6}$$

with the asymptotic covariance matrix $\boldsymbol{\Gamma}_\omega$ of $\boldsymbol{\omega}_i$, $\boldsymbol{\Gamma}_\omega = \lim_{i\to\infty} \mathrm{Cov}(\boldsymbol{\omega}_i) = \left(\frac{\kappa}{2-\kappa}\right) \boldsymbol{\Gamma}$.

The MEWMA control chart triggers an alarm if the control statistic T_i^2 exceeds the threshold value h_4. On in-control data, the statistic (5) is typically reinitialized after a (false) alarm. "In-control" means that only common causes, not special causes like damage, influence the system, while "out-of-control" indicates the presence of special causes such as damage. The in-control "average run length" ARL_0 is used to calibrate the threshold h_4. In general, the ARL is defined as the expected number of observations until the threshold is exceeded. Therefore, the in-control ARL_0 should be high to minimize false alarms, whereas if the process is out-of-control, the ARL (the so-called ARL_1) should be low to detect changes quickly. Since the reconstructed outputs are not independent and identically distributed (i.i.d.) but correlated over time, a simulation-based method is used for calibration. It estimates the ARL by dividing the data into daily blocks and resampling with replacement to create new datasets. In the present study, the ARL is calculated using Eq. (5) and (6) with 100,000 repetitions, and the control limit is chosen to achieve an ARL_0 of 720 (hours), i.e., 30 days. The corresponding algorithm is presented in more detail in [13]. To distinguish the training phase and out-of-sample monitoring, the terms "Phase I" and "Phase II" will be used from now on. Phase I consists only of in-control data, which can be used for model training, whereas Phase II may consist of both in-control and out-of-control data.

4 APPLICATION TO SHM LOAD-TEST DATA

The strain measurements from July 2nd, 2023, to February 17th, 2024, are used as Phase I data to estimate the conditional mean and covariance. The time between February 18th and March 23rd, 2024, will be considered Phase II; this covers the first three additional mass scenarios described above. This data will also be used to calculate the control chart to see whether "damage" (i.e., the additional masses) can be detected. The conditional mean was estimated using penalized regression splines [21, 22]. The optimal bandwidths for the conditional covariance matrix were initially estimated via cross-validation, as described in [12], resulting in small values between 0.1 an 0.3. The conditional covariance was estimated separately for each sensor pair, cf. Eq. (2). Due to the sparse data between 10°C and 15°C, additional smoothing was necessary. To achieve this, the bandwidth was increased to 1.2 to widen the kernel. A wider kernel allows for more data points from adjacent temperatures to be included in the analysis, stabilizing the results. In what follows, the results for three different methods for feature reconstruction will be shown, each utilizing a different type of temperature adjustment:

(a) *Implicit*: This approach uses the common PCA on the measurements, but omits the first principal component when estimating the scores and, subsequently, the reconstructed features. The first principal component is excluded from the estimation because it is assumed to primarily account for operational and environmental effects [17]. This method of temperature compensation is implicit, as it does not require the confounding variable to be measured.

(b) *Partial*: For the partial method, the conditional mean is estimated using penalized regression splines [21, 22]. Then the conditional mean is subtracted from the measurement, i.e., the residuals are calculated, and the marginal mean is added to vertically shift the data to the original scale. Using the conditional mean transforms the partial method into an explicit approach, as it requires the confounder to be measured.

(c) *Conditional*: The conditional method as discussed in Section 3.1 is applied utilizing the conditional mean and the conditional covariance to remove the temperature influence in the mean *and* in the covariance. As with the previous method, the conditional method is an explicit approach that requires measurements of the confounder.

4.1 RECONSTRUCTED STRAIN DATA

Figure 2 shows the original data over time in the first column. The rows correspond to the six strain sensors from Figure 1. The results of implicit feature reconstruction using principal components two to six are found in the second column, the results of the explicit yet partial approach in the third column, and the proposed conditional method in the fourth column. For the latter, all principal components are used. The third column basically shows the residuals obtained by subtracting the estimated conditional mean from the observed data (the first column). The data is colored according to the measured temperature at each time point, i.e., from blue (cold) to red (warm). In the original data, the strain measurements and temperature are highly correlated. This is no longer the case with the reconstructed data; most of the reconstructed outputs appear stable over time and temperature, except for strain sensor 213. Using the partial method, the dependency could not be completely eliminated, although the association is less pronounced than for the original data. All three methods demonstrate the clear advantage of feature reconstruction. By using either (a), (b), or (c) from above, reconstructed data are obtained that align with the original measurements but have been adjusted for temperature. This enables the reconstruction of physically meaningful features without the oscillations caused by EOP in the original data.

For a deeper look, however, Figure 3 shows the Spearman correlations between the reconstructed sensor measurements and the temperature (top), as well as the correlations between the squared differences from the mean $(\tilde{x}_{ij} - \bar{x}_j)^2$ and the temperature. The latter is to detect potential temperature effects on the variance of the reconstructed data, while the former indicates effects on the mean (if so). As can be seen (Figure 3, top), all three methods considered can eliminate temperature dependence regarding the mean (which is very strong in the original data), but if using the partial or particularly the implicit approach, variability tends to increase at least for some strain sensors with increasing temperature (particularly, Str.203 and Str.209 if using the implicit approach).

To further investigate the temperature dependence of the reconstructed data, Figure 4 shows the conditional correlation (top, solid lines) and conditional variance (bottom, solid lines) for a selection of sensor pairs, plotted against temperature, together with the approximate, pointwise

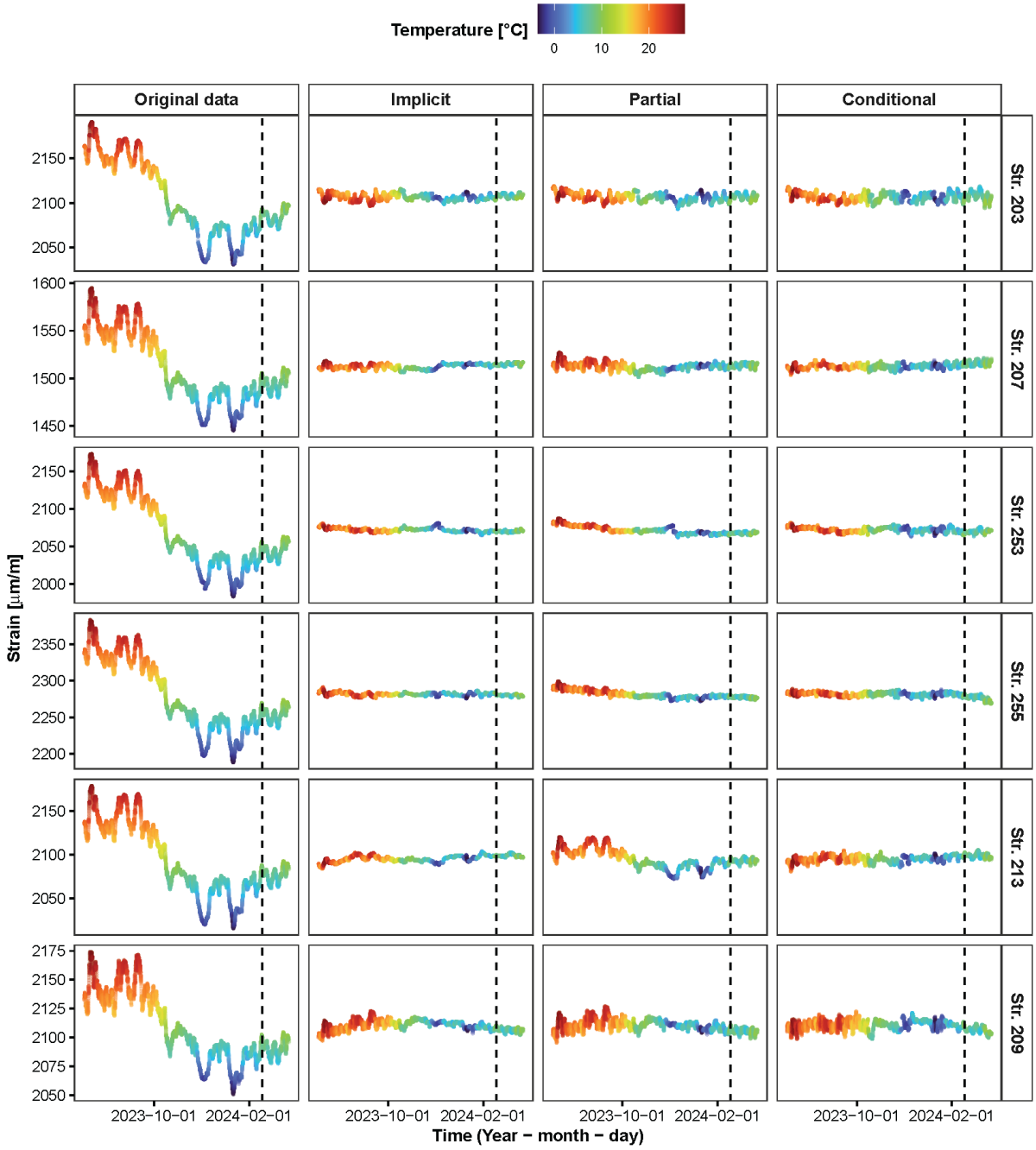


Figure 2: Original strain data (left) from the Vahrendorfer Stadtweg and the reconstructed strain data using the implicit (center left), partial (center right), and conditional (right) methods. The vertical dashed line separates Phase I from Phase II. The data is colored according to the measured temperature.

95% confidence intervals (shaded). The confidence interval was calculated using Eq. (2) and block bootstrapping, as in [13, 29]. Block bootstrapping is used to resample the data by dividing it into blocks of days, followed by estimating the conditional covariance (2). This is repeated 10^5 times to ensure that a comprehensive range of variations is captured. The approximate, pointwise 95% confidence interval is then calculated from the repetitions. A more detailed description is given in [13, 29]. If using the partial method, the temperature dependence is adjusted only in the mean, so the conditional correlations and variances correspond to those of

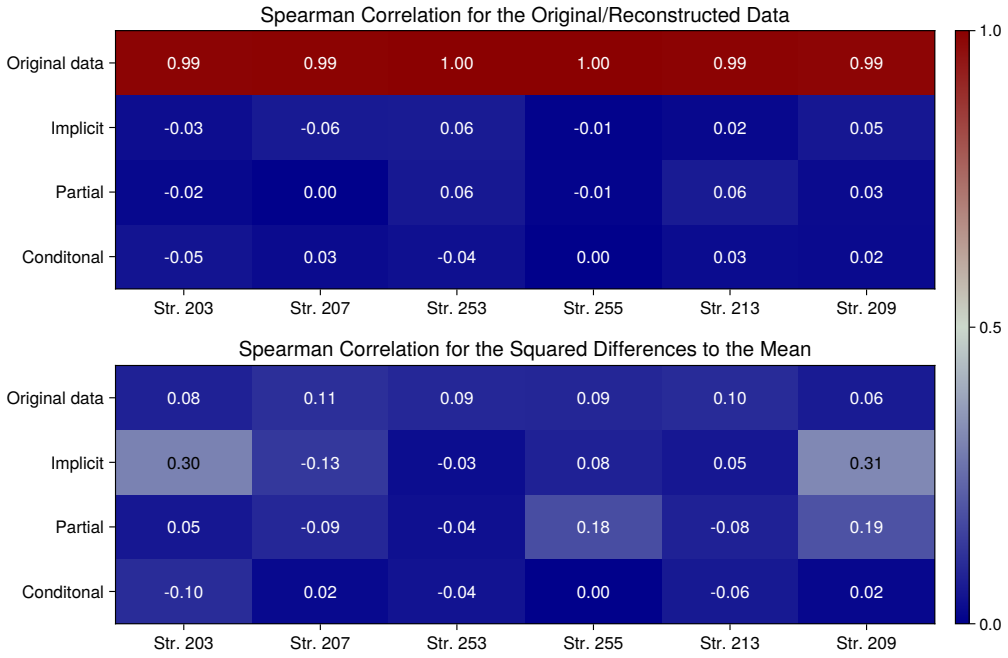


Figure 3: Heatmaps of the Spearman correlation between the original/reconstructed data and the temperature (top panel), and the Spearman correlation between the squared differences of (original/reconstructed) data and the mean and temperature (bottom). In each panel, the first row corresponds to the original data, and the second through fourth rows correspond to the different feature reconstruction methods considered (implicit, partial, and conditional); colors indicate the absolute values of the correlations.

the original measurements; therefore, only the results of the partial method are shown (not for the original data, as they are identical). Those are shown in the second column and vary with different temperatures, indicating that temperature still influences the (co)variance. Omitting the first principal component, i.e., the implicit method (first column), results in a slight improvement regarding the variance but has little to no effect on the correlation. However, the conditional correlations and variances of the reconstructed data remain nearly constant when the newly proposed conditional approach is used, demonstrating that it can eliminate the temperature effect not only in the mean but also in the (co)variance. The confidence intervals in Figure 4 show that most of the estimates are stable across bootstrap samples, but increased uncertainty exists at the boundaries and around 10°C due to sparse data.

4.2 MONITORING RESULTS

The MEWMA control chart (on log scale) from Eq. (5) and (6) is shown in Figure 5 for smoothing parameter $\kappa = 0.2$ and control limits (purple horizontal lines) $h_4 = 175.93$ for the implicit, $h_4 = 165.90$ for the partial, and $h_4 = 125.00$ for the conditional approach. The control limit was estimated using block bootstrapping with the reconstructed data being divided into blocks of days, 10^5 repetitions, and an ARL of $1,000$. The values above the control limit are plotted in red. The dashed vertical line indicates the beginning of Phase II, and the colored areas A, B, and C highlight the three additional mass scenarios (light to heavy).

Two periods of false alarms stand out. For the implicit and partial method, there are false alarms at the beginning of December, when temperatures were low (below 5°C). Here, the control statistic of the conditional method did not trigger the alarm, but in mid-October, when the temperature was around 10°C, it did. The latter false alarms could be due to the sparse

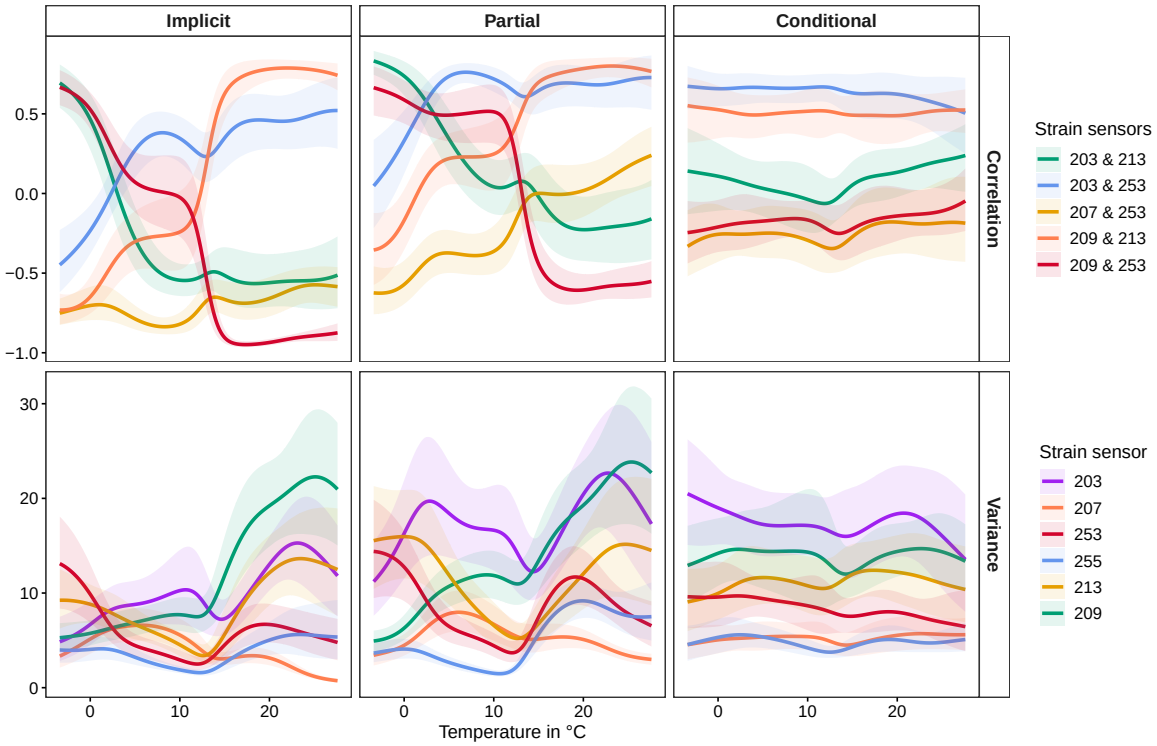


Figure 4: Conditional correlations (top) and variances (bottom) as functions of temperature, together with approximate, pointwise 95% confidence intervals, of the reconstructed strain data from the Vahrendorfer Stadtweg when using the implicit (left), partial (middle), or conditional (right) approach.

training data and, thus, due to an inaccurate estimation of the conditional covariances.

For both the implicit and partial methods, the control statistic does not exceed the control limit at any time in Phase II (after the dashed vertical line). That means the implicit and partial methods failed to detect the additional masses. By contrast, when using the conditional method, the control statistic is almost always above the control limit in the colored areas with added masses, with its height varying across scenarios. The control statistic is lower for the first two additional mass scenarios and higher for the third one. The spike in the control statistic at the beginning of the first scenario can be explained by a car with a trailer and a wheel loader crossing the bridge, which had to be used for repositioning the additional mass.

Table 1 summarizes the Phase I false alarms and the probability of detection for each of the three methods, along with different values of parameter κ. The respective control limits were calculated using block bootstrapping, but the results are similar to those of moving-block bootstrapping. As mentioned in Section 3.2, the parameter κ controls the sensitivity of the shift to be detected. Thus, the values $\kappa = 0.1, 0.3, 1$ were added for comparison. As can be seen again, neither the partial nor the implicit methods can detect the additional masses.

5 SUMMARY AND CONCLUSION

This paper presented a method for calculating confounder-adjusted features from sensor measurements. The reconstructed features are in the same domain as the original measurements, enabling physical interpretation. The presented new approach uses conditional covariances and subsequent (conditional) principal component analysis (PCA) to ensure reliable results and insights. In contrast to standard PCA, the new method requires measuring confounding variables,

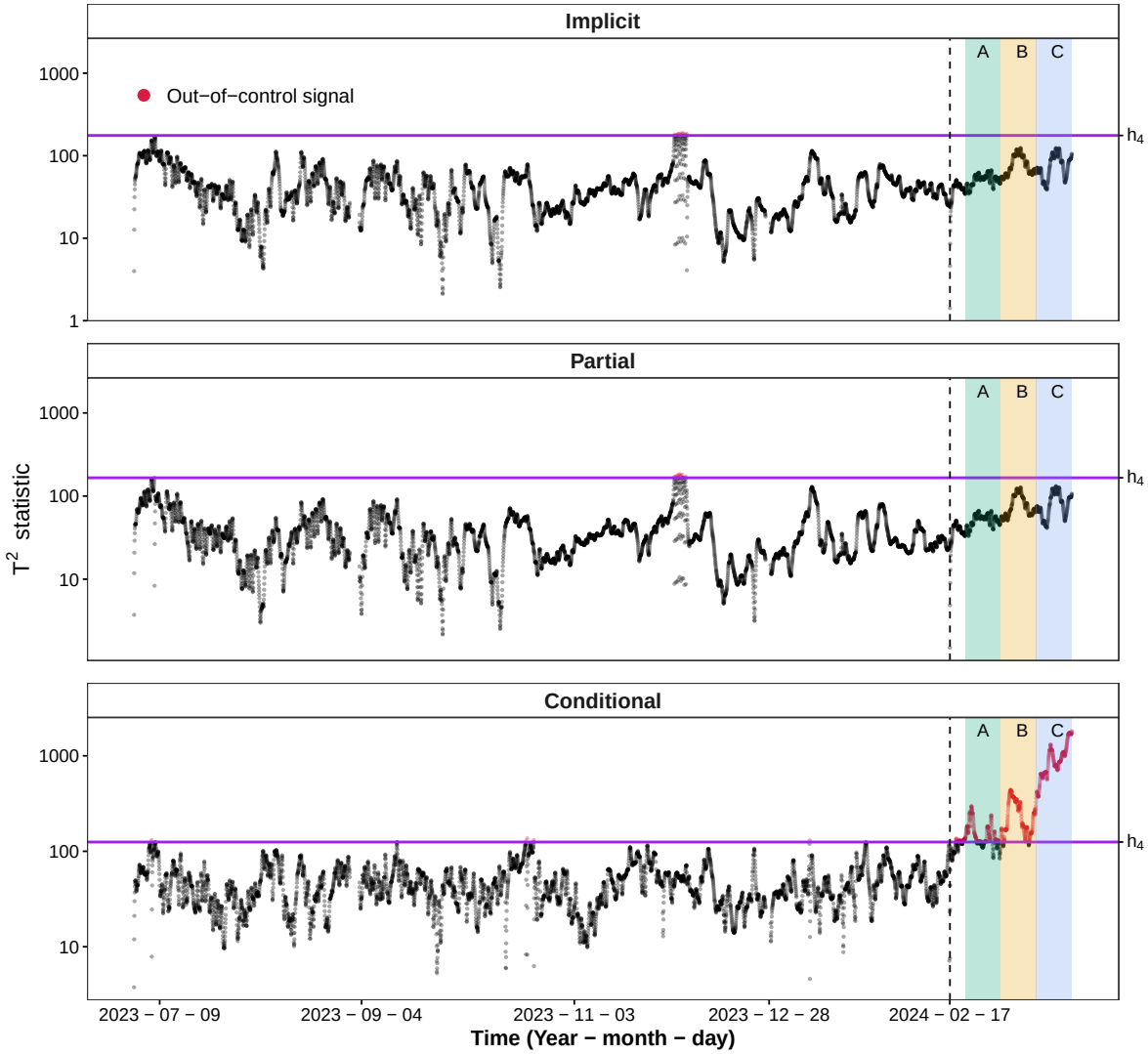


Figure 5: MEWMA control chart (with $\kappa = 0.2$) on log scale for the implicit ($h_4 = 175.93$), partial ($h_4 = 165.90$), and conditional ($h_4 = 125.00$) approaches for feature reconstruction for the Vahrendorfer Stadtweg strain data. The control limits h_4 are calculated using block bootstrapping. The dashed line separates Phase I from Phase II, with the three load test scenarios highlighted in color.

such as environmental and operational parameters, thus transforming PCA from an implicit to an explicit method. Considering a real-world bridge dataset, the reconstructed features showed no dependence on temperature in either the mean or the (co-)variance anymore. Existing approaches for confounder removal (e.g., omitting the first principal component or response surface modeling), by contrast, could not fully eliminate the influence of the confounding variable. This was especially noticeable in the conditional (co-)variances. While temperature dependencies in the mean could be removed, covariances still varied (non-linearly) with temperature.

Limitations of the new, conditional approach include the need to measure confounding variables both during the in-control phase to ensure reliable training, as demonstrated with the Vahrendorfer Stadtweg bridge (where infrequent temperature measurements led to unreliable or no reconstructed features), and during the entire monitoring phase.

Additionally, an advanced multivariate control chart, the MEWMA control chart, was established to monitor the reconstructed features and determine whether damage could be detected.

Table 1: Phase I false alarms and the probability of detection (POD) per method and varying smoothing parameter κ for the bridge Vahrendorfer Stadtweg. The respective control limits h_4 were calculated using block bootstrapping.

	Implicit			**Partial**			**Conditional**		
κ	False Alarms		POD	False Alarms		POD	False Alarms		POD
0.1	**7**	[**0.13**%]	0%	9	[0.17%]	0%	12	[0.22%]	**100**%
0.2	9	[0.17%]	0%	11	[0.20%]	0%	**6**	[**0.11**%]	**87.4**%
0.3	12	[0.22%]	0%	15	[0.28%]	0%	**6**	[**0.11**%]	**75.73**%
1.0	85	[1.57%]	0%	92	[1.70%]	0%	**21**	[**0.39**%]	**64.08**%

To evaluate the performance of the considered methods, two factors were examined: the false alarm rate and the probability of detection. The striking result was that the probability of detection could be increased to 64%-100% when using the conditional approach, compared to 0% for the common implicit and partial methods. In other words, only the new conditional approach detected the additional masses, especially the lightest, whereas the implicit and partial methods failed to detect even the heaviest mass.

CODE AVAILABILITY

Code implementing the output reconstruction and the monitoring procedure is available on GitHub at `https://github.com/neumannLizzie/FeatureReconstructionSHM/`.

ACKNOLEDGMENTS

This research paper out of the project “SHM – Digitalisierung und Überwachung von Infrastrukturbauwerken” is funded by dtec.bw – Digitalization and Technology Research Center of the Bundeswehr, which we gratefully acknowledge. dtec.bw is funded by the European Union – NextGenerationEU.

REFERENCES

[1] Charles Farrar and Keith Worden. *Structural Health Monitoring: A Machine Learning Perspective*. John Wiley & Sons, Ltd, 2013. DOI: 10.1002/9781118443118.

[2] Onur Avci et al. “A review of vibration-based damage detection in civil structures: From traditional methods to Machine Learning and Deep Learning applications”. In: *Mechanical Systems and Signal Processing* 147 (2021), p. 107077. DOI: 10.1016/j.ymssp.2020.107077.

[3] Qinghua Han et al. “Structural health monitoring research under varying temperature condition: a review”. In: *Journal of Civil Structural Health Monitoring* 11 (2021), pp. 149–173. DOI: 10.1007/s13349-020-00444-x.

[4] Zhen Wang et al. “Eliminating environmental and operational effects on structural modal frequency: A comprehensive review”. In: *Structural Control and Health Monitoring* 29.11 (2022), e3073. DOI: 10.1002/stc.3073.

[5] Filipe Magalhães, Álvaro Cunha, and E. De Sá Caetano. “Vibration based structural health monitoring of an arch bridge: From automated OMA to damage detection”. In: *Mechanical Systems and Signal Processing* 28 (2012), pp. 212–228. DOI: 10.1016/j.ymssp.2011.06.011.

[6] Edwin Reynders, Gersom Wursten, and Guido De Roeck. "Output-only structural health monitoring in changing environmental conditions by means of nonlinear system identification". In: *Structural Health Monitoring* 13.1 (2014), pp. 82–93. DOI: 10.1177/1475921713502836.

[7] Keith Worden, Graeme Manson, and Cecilia Surace. "Aspects of novelty detection". In: *Key Engineering Materials* 347 (2007), pp. 3–16. DOI: 10.4028/www.scientific.net/KEM.347.3.

[8] Alireza Entezami, Hashem Shariatmadar, and Carlo De Michele. "Non-parametric empirical machine learning for short-term and long-term structural health monitoring". In: *Structural Health Monitoring* 21.6 (2022), pp. 2700–2718. DOI: 10.1177/14759217211069842.

[9] Michael Döhler et al. "Structural health monitoring with statistical methods during progressive damage test of S101 Bridge". In: *Engineering Structures* 69 (2014), pp. 183–193. DOI: 10.1016/j.engstruct.2014.03.010.

[10] Yi Qing Ni et al. "Correlating modal properties with temperature using long-term monitoring data and support vector machine technique". In: *Engineering Structures* 27.12 (2005), pp. 1762–1773. DOI: 10.1016/j.engstruct.2005.02.020.

[11] Alexandre Cury, Christian Cremona, and John Dumoulin. "Long-term monitoring of a PSC box girder bridge: Operational modal analysis, data normalization and structural modification assessment". In: *Mechanical Systems and Signal Processing* 33 (2012), pp. 13–37. DOI: 10.1016/j.ymssp.2012.07.005.

[12] Lizzie Neumann et al. "Confounder-adjusted covariances of system outputs and applications to structural health monitoring". In: *Mechanical Systems and Signal Processing* 224 (2025), p. 111983. DOI: 10.1016/j.ymssp.2024.111983.

[13] Lizzie Neumann et al. "Signal and Feature Reconstruction in Structural Health Monitoring under Varying Environmental Conditions". In: *Engineering Structures* 361 (2026), p. 122865. DOI: 10.1016/j.engstruct.2026.122865.

[14] Martin Köhncke et al. "Data Set of Load Tests and Structural Health Monitoring of a concrete boxgirder bridge". In: *Preprint, arXiv:2412.15713* (2026). DOI: 10.48550/arXiv.2412.15713. arXiv: 2412.15713 [stat.AP].

[15] Diego A Tibaduiza et al. "Structural damage detection using principal component analysis and damage indices". In: *Journal of Intelligent Material Systems and Structures* 27.2 (2016), pp. 233–248. DOI: 10.1177/1045389X14566520.

[16] Yanjie Zhu et al. "A temperature-driven MPCA method for structural anomaly detection". In: *Engineering Structures* 190 (2019), pp. 447–458. DOI: 10.1016/j.engstruct.2019.04.004.

[17] Elizabeth J. Cross et al. "Features for damage detection with insensitivity to environmental and operational variations". In: *Proceedings of the Royal Society A* 486 (2012), pp. 4098–4122. DOI: 10.1098/rspa.2012.0031.

[18] Kundan Kumar, Prabir Kumar Biswas, and Nirjhar Dhang. "Time series-based SHM using PCA with application to ASCE benchmark structure". In: *Journal of Civil Structural Health Monitoring* 10 (2020), pp. 899–911. DOI: 10.1007/s13349-020-00423-2.

[19] Lizzie Neumann. "Monitoring Confounder-adjusted Principal Component Scores with an Application to Load Test Data". In: *Proceedings of the 35th European Safety and Reliability & the 33rd Society for Risk Analysis Europe Conference*. Ed. by Eirik Bjorheim Abrahamsen et al. Singapore: Research Publishing, 2025, pp. 2985–2992. DOI: 10.3850/978-981-94-3281-3_ESREL-SRA-E2025-P5913-cd.

[20] Jianxin Yin et al. "Nonparametric covariance model". In: *Statistica Sinica 20* (2010), pp. 469–479.

[21] Paul H. C. Eilers and Brian D. Marx. "Flexible smoothing with B-splines and penalties". In: *Statistical Science* 11.2 (1996), pp. 89–121. DOI: 10.1214/ss/1038425655.

[22] Lizzie Neumann and Jan Gertheiss. "Covariate-adjusted Association of Sensor Outputs for Structural Health Monitoring". In: *dtec.bw-Beiträge der Helmut-Schmidt-Universität / Universität der Bundeswehr Hamburg*. Ed. by D. Schulz et al. Vol. 1. 2022, pp. 287–291. DOI: 10.24405/14566.

[23] William S. Cleveland, Eric Grosse, and William M. Shyu. "Local regression models". In: *Statistical models in S*. Routledge, 2017, pp. 309–376.

[24] Alexander Petersen, Sean Deoni, and Hans-Georg Müller. "Fréchet estimation of time-varying covariance matrices from sparse data, with application to the regional co-evolution of myelination in the developing brain". In: *The Annals of Applied Statistics* 13.1 (2019), pp. 393–419. DOI: 10.1214/18-AOAS1195.

[25] Cynthia A. Lowry et al. "A Multivariate Exponentially Weighted Moving Average Control Chart". In: *Technometrics* 34.1 (1992), pp. 46–53. DOI: 10.2307/1269551.

[26] Sven Knoth. "ARL Numerics for MEWMA Charts". In: *Journal of Quality Technology* 49.1 (2017), pp. 78–89. DOI: 10.1080/00224065.2017.11918186.

[27] John Stuart Hunter. "The Exponentially Weighted Moving Average". In: *Journal of Quality Technology* 18.4 (1986), pp. 203–210. DOI: 10.1080/00224065.1986.11979014.

[28] Harold Hotelling. "Multivariate quality control illustrated by the air testing of sample bombsights". In: *Techniques of Statistical Analysis*. Ed. by C. Eisenhart, M.W. Hastay, and W.A. Wallis. New York: McGraw-Hill, 1947, pp. 111–184.

[29] Lizzie Neumann, Philipp Wittenberg, and Jan Gertheiss. "Confidence Intervals for Conditional Covariances of Natural Frequencies". In: *Proceedings of the 11th International Operational Modal Analysis Conference (IOMAC 2025)*. Ed. by M. Döhler, A. Mélot, and M. A. López. Rennes, France, 2025, pp. 742–749. ISBN: 978-84-09-75120-4.